

vegetation on extrasolar terrestrial planets, but photometric measurements in different colours may be able to detect a unique signature, different from any known surface features or atmospheric constituents on Earth or other solar system planets.

We expect the diurnal rotational variation of an Earth-like planet to be lower in the mid-infrared (flux variation of a few per cent) than in the optical because the surface temperature does not vary as much as surface albedo across the Earth. For a planet with non-zero obliquity the mid-infrared seasonal flux variation should be larger than the mid-infrared rotational variation because of seasonal temperature variation. In addition, optical multicolour photometry and polarization as a function of phase angle (on an orbital timescale) could help constrain the type of atmospheric scatterers and the particle size distribution or detect a large smooth specular surface such as an ice- or an ocean-covered planet. Alternatively, the variation on an orbital timescale may be overwhelmed by variations indicating strong seasonal changes in the atmosphere.

Theoretical light curves of the unresolved Earth have a variation of 10–20%. A terrestrial planet finder that can measure 5% optical variation could detect weather, the rotational period, and seasonal changes in the cloud pattern of a planet like our Earth. If the surface were to contribute most of the scattered light rather than the clouds, then planets with different surface features would show very different diurnal light curves. This is in dramatic contrast to planets like Venus which would show almost no diurnal variability. Thus, we expect the diurnal light curve of an extrasolar Earth-like planet to contain detectable features encoding information about its physical and perhaps even biological properties. □

Received 17 April; accepted 9 July 2001.

1. Marcy, G. W., Cochran, W. D. & Mayor, M. in *Protostars and Planets IV* (eds Mannings, V., Boss, A. P., Russell, S. S.) 1285–1311 (Univ. Arizona Press, Tucson, 2000).
2. Butler, R. P., Marcy, G. W., Williams, E., McCarthy, C. & Dopsanjh, P. Attaining Doppler precision of  $3 \text{ m s}^{-1}$ . *Proc. Astron. Soc. Pacif.* **108**, 500–509 (1996).
3. Beichman, C. A., Woolf, N. J. & Lindensmith, C. A. The terrestrial planet finder (TPF). *NASA/JPL Publ.* **99-3**, 1–22 (1999).
4. Darwin the infrared space interferometer—concept and feasibility study report. Technical Report ESA-SCI(2000)12, 1–85 (European Space Agency, 2000).
5. Nisenson, P. & Pappaloulos, C. Detection of earth-like planets using apodized telescopes. *Astrophys. J.* **548**, L201–205 (2001).
6. Spergel, D. N. A new pupil for detecting extrasolar planets. *Appl. Optics* (submitted); also preprint astro-ph/0101142 at (xxx.lanl.gov) (2001).
7. Schindler, T. L. & Kasting, J. F. Synthetic spectra of simulated terrestrial atmospheres containing possible biomarker gases. *Icarus* **145**, 262–271 (2000).
8. Brown, T. M., Charbonneau, D., Gilliland, R. L., Noyes, R. W. & Burrows, A. Hubble Space Telescope time-series photometry of the transiting planet of HD 209458. *Astrophys. J.* **552**, 699–709 (2001).
9. Hapke, B. *Theory of Reflectance and Emittance Spectroscopy* (Cambridge Univ. Press, Cambridge, 1993).
10. Bukata, R. P., Jerome, J. H., Kondratyev, K. Ya. & Pozdnyakov, D. V. *Optical Properties and Remote Sensing of Inland and Coastal Waters* 37–102 (CRC Press, New York, 1995).
11. Vokrouhlicky, D. & Farinella, P. Specular reflection of sunlight from wavy ocean surfaces and the albedo effect on satellite orbits I. A statistical model. *Astron. Astrophys.* **293**, 307–322 (1995).
12. Jerome, J. H., Bukata, R. P. & Bruton, J. E. Utilizing the components of vector irradiance to estimate the scalar irradiance in natural waters. *Appl. Optics* **27**, 4012–4018 (1988).
13. Kirk, J. T. O. Volume scattering function, average cosines, and the underwater light field. *Limnol. Oceanogr.* **36**, 455–467 (1991).
14. Bricaud, A., Babin, M., Morel, A. & Claustre, H. Variability in the chlorophyll-specific absorption coefficients of natural phytoplankton: analysis and parameterization. *J. Geophys. Res.* **100**, 13321–13332 (1995).
15. Kondratyev, K. Ya. *Radiation in the Atmosphere* (Academic, New York, 1969).
16. Verbiscer, A. J. & Veverka, J. Scattering properties of natural snow and frost: comparison with icy satellite photometry. *Icarus* **88**, 418–428 (1990).
17. Myneni, R. B. *et al.* Optical remote sensing of vegetation: modeling, caveats, and algorithms. *Remote Sens. Environ.* **51**, 169–188 (1995).
18. Jacquemoud, S., Baret, F. & Hanocq, J. F. Modeling spectral and bidirectional soil reflectance. *Remote Sens. Environ.* **41**, 123–132 (1992).
19. Woessner, P. & Hapke, B. Polarization of light scattered by clover. *Remote Sens. Environ.* **21**, 243–261 (1987).
20. DeFries, R. S. & Townshend, J. R. G. NDVI-derived land cover classification at a global scale. *Int. J. Remote Sens.* **15**, 3567–3586 (1994).
21. Hovenier, J. W. & Hage, J. I. Relations involving the spherical albedo and other photometric quantities of planets with thick atmospheres. *Astron. Astrophys.* **214**, 391–401 (1989).
22. Rossow, W. B. & Schiffer, R. A. ISCCP cloud data products. *Bull. Am. Meteorol. Soc.* **72**, 2–20 (1991).
23. Goode, P. R. *et al.* Earthshine Observations of the Earth's Reflectance. *J. Geophys. Res. Lett.* **28**, 1671–1674 (2001).

24. Sagan, C., Thompson, W. R., Carlson, R., Gurnett, D. & Hord, C. A. Search for life on earth from the Galileo spacecraft. *Nature* **365**, 715 (1993).

**Acknowledgements**

We thank the members of the Ball Aerospace Terrestrial Planet Finder team, B. Soden, A. Broccoli and G. Williams for discussions, and B. Soden for assistance with the ISCCP database. We wish to thank W. B. Rossow, the Goddard Institute for Space Studies, the Goddard Space Flight Center, and NASA for the production and distribution of this data set. E.B.F. would like to acknowledge support under a National Science Foundation Graduate Fellowship and S.S. is supported by the W. M. Keck Foundation.

Correspondence and requests for materials should be addressed to E.B.F. (e-mail: eford@astro.princeton.edu).

**Stimulated emission of polarization-entangled photons**

**A. Lamas-Linares, J. C. Howell & D. Bouwmeester**

*Centre for Quantum Computation, Clarendon Laboratory, University of Oxford, Parks Road, Oxford OX1 3PU, UK*

Entangled photon pairs—discrete light quanta that exhibit non-classical correlations—play a crucial role in quantum information science (for example, in demonstrations of quantum non-locality<sup>1–7</sup>, quantum teleportation<sup>8,9</sup> and quantum cryptography<sup>10–12,31</sup>). At the macroscopic optical-field level non-classical correlations can also be important, as in the case of squeezed light<sup>13</sup>, entangled light beams<sup>14,15</sup> and teleportation of continuous quantum variables<sup>16</sup>. Here we use stimulated parametric down-conversion to study entangled states of light that bridge the gap between discrete and macroscopic optical quantum correlations. We demonstrate experimentally the onset of laser-like action for entangled photons, through the creation and amplification of the spin-1/2 and spin-1 singlet states consisting of two and four photons, respectively. This entanglement structure holds great promise in quantum information science where there is a strong demand for entangled states of increasing complexity.

As the acronym LASER (light amplification by stimulated emission of radiation) indicates, polarization-entangled laser operation would mean that a (spontaneously created) photon pair in two polarization-entangled modes stimulate, inside a nonlinear gain medium, the emission of additional pairs. As a gain medium we consider type-II parametric down-conversion<sup>17</sup>. A simplified interaction hamiltonian<sup>18,19</sup> for the nonlinear interaction between a classical pump field and two polarization-entangled modes *a* and *b* is given by

$$\hat{H}_{\text{int}} = e^{i\phi} \kappa \hat{K}^{\dagger} + e^{-i\phi} \kappa \hat{K} \tag{1}$$

where  $\hat{K}^{\dagger} \equiv (\hat{a}_H^{\dagger} \hat{b}_V^{\dagger} - \hat{a}_V^{\dagger} \hat{b}_H^{\dagger})$  and  $\hat{K} \equiv (\hat{a}_H \hat{b}_V - \hat{a}_V \hat{b}_H)$  are the creation and annihilation operators of polarization-entangled photon pairs in modes *a* and *b*. Horizontal and vertical polarization are represented by H and V, and  $\kappa$  is a real-valued coupling coefficient. When acting on the vacuum state the time evolution operator  $\hat{U} = \exp(i\hat{H}t/\hbar)$  yields:

$$|\psi\rangle \propto \sum_{n=0}^{\infty} (\tanh \tau)^n \sum_{m=0}^n (-1)^m |n - m, m; m; n - m\rangle \tag{2}$$

where  $\tau \equiv \kappa t/\hbar$  is the interaction parameter. The first and second positions in the ket indicate respectively the number of horizontal (*n - m*) and vertical (*n*) photons in mode *a*, and the third and fourth positions indicate the corresponding numbers for mode *b*. This state represents the general output of type-II parametric down-

conversion, but for all experiments reported to date,  $\tau$  is so small that mainly the first-order term ( $n = 1$ ) has been taken into account and only a few experiments and proposals have addressed second-order terms<sup>7,20–24</sup>. By analogy with a conventional laser, the idea of an entangled-photon laser is to increase  $\tau$  using a resonator around the gain medium, which enhances the emission of the higher-order terms in equation (2). The state shown in equation (2) has the following features.

First, modes  $a$  and  $b$  are entangled in photon number because, for any  $n$ , the number of photons in each mode is identical. The photon (pair) number distribution is shown in Fig. 1 for increasing average photon (pair) number output per pulse  $\langle n \rangle$ . The shifting of the maximum and the broadening of the distribution for higher values of  $\langle n \rangle$  resembles the coherent state photon-number distribution as produced by conventional lasers. These features are explained by the fact that stimulated emission—originating from the boson statistics of photons—favours amplification of higher over lower photon-number terms.

The second important property of the state in equation (2) is that the set of terms for each  $n$  form a maximally entangled state in polarization. The normalized 1-pair term is the rotationally symmetric Bell state (singlet spin-1/2):

$$|\psi\rangle = \frac{1}{\sqrt{2}}(|1, 0; 0, 1\rangle - |0, 1; 1, 0\rangle) \quad (3)$$

The normalized 2-pair term is given by

$$|\psi\rangle = \frac{1}{\sqrt{3}}(|2, 0; 0, 2\rangle - |1, 1; 1, 1\rangle + |0, 2; 2, 0\rangle) \quad (4)$$

and represents the singlet spin-1 state. Similar to the spin-1/2 case, the rotational symmetry arises from the relative phase relations and the equal weights of the terms. In general, the  $n$ -pair term has the properties of a singlet spin- $n/2$  state. The rotational symmetry of the full state can be shown by expressing the  $n$ -pair terms in any other basis, and verifying that the same expressions are obtained. The crucial role of stimulated emission is to provide for each  $n$  equally weighted terms. In principle, a photon counting measurement on state (2) (either in mode  $a$  or  $b$ ) performs a projection onto a certain singlet spin- $n/2$  state. Subsequently, this maximally entangled state can be explored for quantum information tasks. In practice, in quantum optics experiments where the fragile photons are in general destroyed by any measurement, the projection and the exploration of the state are performed simultaneously. This procedure, usually referred to as post-selection, has proved to be very useful: for example, for demonstrations of quantum teleportation<sup>8</sup>,

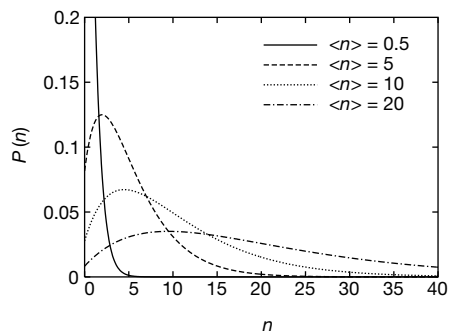


**Figure 1** The photon number (pair) distribution,  $P(n)$ , arising from stimulated parametric down-conversion shifts its peak and broadens as the mean number of photons increases. This indicates that for increasing interaction strength (gain), terms with higher numbers of photons obtain a larger amplification factor compared to lower terms, which is a feature of laser operation.

quantum cryptography<sup>10–12,31</sup>, and three-particle Greenberger–Horne–Zeilinger (GHZ) correlations<sup>7,21</sup>, and for novel optical quantum computation schemes<sup>25</sup>. Here we use post-selection to demonstrate stimulated entanglement by measuring 2- and 4-photon properties of state (2) for increasing values of  $\tau$ .

The set-up used to demonstrate stimulated entanglement is illustrated in Fig. 2. A 120-fs pump pulse at 390 nm wavelength (with a repetition rate of 80 MHz) passes through a  $\beta$ -barium borate (BBO) crystal and creates pairs of polarization-entangled photons in spatially distinct modes  $a$  and  $b$ . The experimental parameters are chosen such that (to first order) the singlet photon-pair state shown in equation (3) is created. Initially modes  $a$  and  $b$  are in the vacuum state and the photon pairs are spontaneously created. The fact that modes  $a$  and  $b$  geometrically diverge, and that horizontally and vertically polarized photons experience different crystal parameters, limits the useful crystal length<sup>26</sup> and thereby prohibits an efficient stimulated emission process. To obtain significant stimulated emission we redirect the spontaneously created photon pairs into the crystal at the same time (tuned by a delay on mirror M3) as the reflected pump pulse passes through the crystal a second time. Provided that the feedback loop for the photon pairs is polarization independent, which is obtained by using a bow-tie folded geometry including a  $\lambda/2$  waveplate that exchanges H and V polarizations, optimum conditions for stimulated emission of photon pairs can be established. As stimulated emission can be seen as a constructive multi-particle interference effect, and because the process of parametric down-conversion is sensitive to the phase of the pump, we should expect to observe an oscillation between stimulation and suppression of emission as function of the pump-pulse delay. The period of this oscillation corresponds to the optical frequency of the pump laser. In the region where the difference between the pump delay and the feedback loop is larger than the coherence length of the observed photons (determined by the 5-nm narrow-bandwidth filters in front of the single-photon detectors), no such interference pattern is expected.

To study the 2- and 4-photon entangled states we measure each term in equations (3) and (4) individually in two non-orthogonal polarization bases. The  $|1,0;0,1\rangle$  and the  $|0,1;1,0\rangle$  terms are measured in the desired bases by using a polarizer in front of a single-photon detector in each of the spatial modes  $a$  and  $b$ . The  $|1,1;1,1\rangle$  term is detected by the introduction of polarizing beam splitters in the appropriate basis in each mode followed by four single-photon detectors (Fig. 2). As we do not use multi-photon detectors, we can

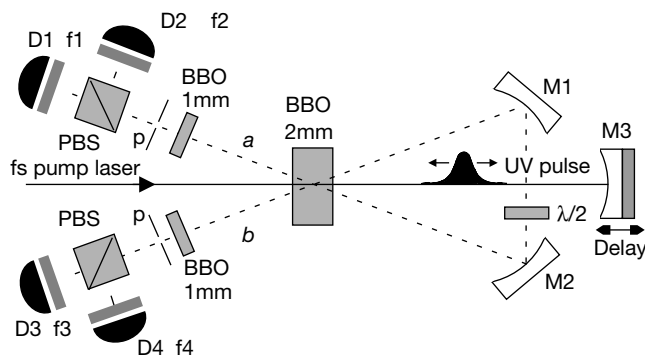


**Figure 2** Experimental set-up. A frequency-doubled, mode-locked Ti:sapphire laser (80 MHz repetition rate,  $\lambda = 390$  nm) pumps a 2-mm (BBO)  $\beta$ -barium borate crystal. Pinholes (p) perform spatial selection of the entangled modes. The pump is reflected onto itself by mirror M3 that is mounted on a computer-controlled translation stage. Mirrors M1 and M2 form the feedback loop, including a polarization rotation element ( $\lambda/2$ ), for the entangled photons. Photon detection of the  $|1,1;1,1\rangle$  term in the H/V basis occurs at avalanche photodiodes D1–D4, after going through polarizing beam splitters (PBS) and 5-nm-bandwidth filters f1–f4. The role of the two extra 1-mm BBO crystals in modes  $a$  and  $b$  is to compensate for undesirable birefringent properties of the main crystal<sup>17</sup>.

only measure the  $|2,0;0,2\rangle$  and the  $|0,2;2,0\rangle$  term with a 0.25 probability using a combination of a polarizer, a 50-50 beam splitter and two single-photon detectors in each mode.

Quantitative predictions for the amplification of the individual terms in equations (3) and (4) resulting from the double-pass configuration are obtained by expanding the unitary evolution of the created light fields in the polarization-entangled photon-pair creation operator  $\hat{K}^\dagger$ . To second order in  $\hat{K}^\dagger$  we obtain

$$\hat{U} = \hat{U}_2 \hat{U}_1 = 1 + e^{i\theta} \tau \hat{K}_2^\dagger + \tau \hat{K}_1^\dagger + \frac{1}{2} e^{2i\theta} \tau^2 (\hat{K}_2^\dagger)^2 + \frac{1}{2} \tau^2 (\hat{K}_1^\dagger)^2 + e^{i\theta} \tau^2 \hat{K}_2^\dagger \hat{K}_1^\dagger \quad (5)$$

where subscripts 1 and 2 refer to the first and second pass through

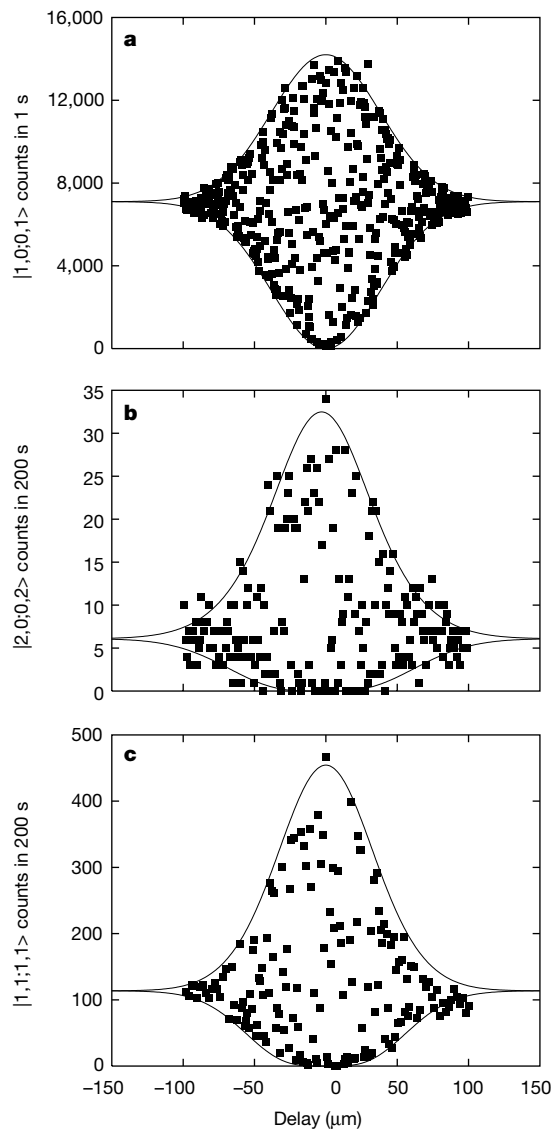


**Figure 3** Experimental demonstration of stimulated entanglement. **a**, The 2-fold coincidence rate corresponding to the detection of the  $|1,0;0,1\rangle$  term in the  $45^\circ$  rotated basis as function of the delay between the reflected pump and the entangled photons generated in the first pass through the crystal. Solid lines, theoretical fits to the envelope of the curve as the degree of overlap varies. **b**, The 4-fold coincidence rate corresponding to the detection of the  $|2,0;0,2\rangle$  term in the  $45^\circ$  rotated basis, and **c**, the  $|1,1;1,1\rangle$  in the H/V basis. The effect of stimulated emission is apparent in the increase of the number of 4-fold coincidences at zero delay of a factor of 5.3 and 4.0 for the  $|2,0;0,2\rangle$  and  $|1,1;1,1\rangle$  terms, respectively (see text). The difference in rates between the two 4-photon graphs is due to the probabilistic detection and extra elements introduced to measure the  $|2,0;0,2\rangle$  term.

the crystal. The relative phase  $\theta$  between the first and second pass of the pump pulse is tunable by the translation of mirror M3 (Fig. 2). We discuss two limits: when  $\hat{K}_1^\dagger = \hat{K}_2^\dagger$ , and when  $\hat{K}_1^\dagger$  is distinguishable from  $\hat{K}_2^\dagger$ . The first case applies at zero delay where efficient phase-sensitive stimulated emission occurs. From equation (5) it follows that doubling the value of the interaction parameter  $\tau$  results in an increase in probability for the 2-photon terms from  $\tau^2$  to  $4\tau^2$ , and in an increase for the 4-photon terms from  $\tau^4$  to  $16\tau^4$ . We note that the 4-photon state has a four times larger amplification than the 2-photon states, which is characteristic of stimulated emission. The second case applies if the reflected pump-pulse delay between the two passes is not equal to the delay of the entangled photons in the feedback loop. In this case, there are simply two independent contributions to the 2-photon detection events, but there are several distinct contributions to the 4-photon detection events. Each single pass has a small probability (of  $\tau^4$ ) to create state (4). In addition, as current single-photon detectors do not have a high enough time resolution to distinguish between photons arriving from the first or second pass, there are spurious 4-fold coincidences from a combination of 2-photon states created in both passes. The spurious contributions to the  $|2,0;0,2\rangle$  and the  $|0,2;2,0\rangle$  detections will be  $\tau^4$ , and for the  $|1,1;1,1\rangle$  detection will be  $2\tau^4$ .

We scan from the region where  $\hat{K}_1^\dagger$  is completely distinguishable from  $\hat{K}_2^\dagger$  into the region where  $\hat{K}_1^\dagger = \hat{K}_2^\dagger$ , while observing the intensity of the 2- and 4-photon terms. From the considerations above we expect—in the case of ideal stimulated emission—the terms in equation (3) to show a 2-fold increase, the middle term in equation (4) to show a 4-fold increase, and the other two terms in equation (4) to increase by a factor of  $16/3 = 5.33$ . Owing to the rotational symmetry of states (3) and (4), these predictions are basis independent.

Figure 3 shows our experimental data for the detection of the  $|1,0;0,1\rangle$  (panel a) and the  $|2,0;0,2\rangle$  (b) terms measured in the  $45^\circ$

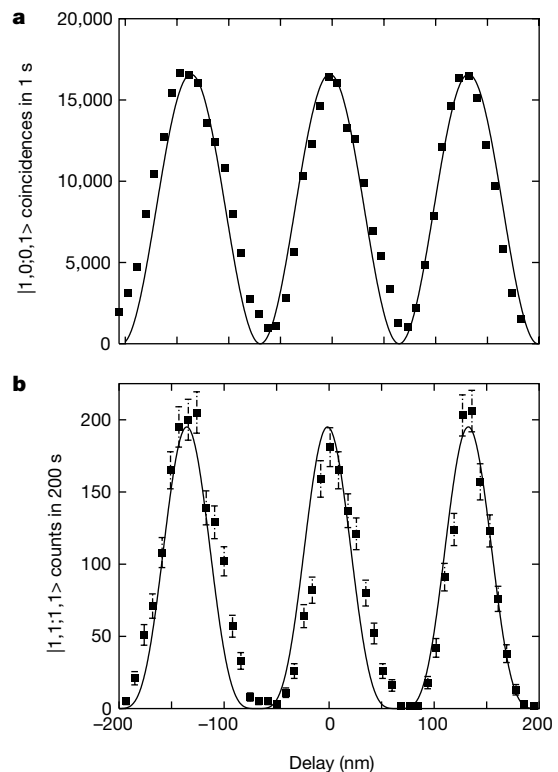


**Figure 4** Two- and four-photon interference due to stimulated emission. A fine scan of the  $|1,0;0,1\rangle$  (**a**) and  $|1,1;1,1\rangle$  (**b**) terms in the zero-delay region shows optimum stimulation and suppression of the 2- and 4-fold coincidence probability.

rotated basis, and the  $|1,1;1,1\rangle$  (c) term in the H/V basis. The solid curves are the envelopes of the oscillating functions giving the maximum and minimum theoretical values for the coincidence rates. The experimental data show an increase of  $1.95 \pm 0.10$  for  $|1,0;0,1\rangle$ ,  $5.3 \pm 0.6$  for  $|2,0;0,2\rangle$  and of  $4.1 \pm 0.3$  for  $|1,1;1,1\rangle$ . These results are in good agreement with the predictions discussed above. Similar results have been obtained in the other bases and for the  $|0,1;1,0\rangle$  and  $|0,2;2,0\rangle$  terms, demonstrating the rotational invariance—that is, the spin-1/2 and spin-1 singlet structure—of states (3) and (4). Additional data indicate an amplification due to the second pass of  $3.95 \pm 0.10$  for the 2-fold coincidences, and of  $17 \pm 2$  for the 4-fold coincidences. This demonstrates the shifting of the photon-number pair distribution towards terms with higher photon numbers, a characteristic of stimulated emission. A final proof of stimulated emission—seen as a constructive interference process—is the phase-dependent emission probability shown in Fig. 4. This is a fine scan around the region of zero delay for the  $|1,0;0,1\rangle$  (panel a) and the  $|1,1;1,1\rangle$  (b) terms in the  $45^\circ$  rotated basis and H/V basis, respectively. The solid lines are fits to the theoretical predictions, which vary as  $(1 + \cos\theta)$  for the 2-photon case, and as  $(1 + \cos\theta)^2$  for the 4-photon case. The visibility of these interference fringes is in all cases above 97%.

In summary, we have pointed out that the rich entanglement structure—equivalent to a superposition of spin- $n/2$  singlet states—obtained by stimulated emission of the familiar rotationally symmetric Bell state; we have also demonstrated that stimulated emission of polarization-entangled photons can be achieved experimentally. Both the characteristic shifting of the photon pair distribution towards higher photon numbers, and the rotational symmetry of the 2- and 4-photon contribution, have been observed. The good agreement between the experimental data and the theory shows that the stringent indistinguishability requirements to obtain entanglement in a stimulated process using external resonators have been met. Although related theory and experiments on interference-enhanced emission of photon pairs and on photon injection into nonlinear crystals have been reported<sup>22,23,27,28</sup>, our results constitute (to our knowledge) the first experimental demonstration of the onset of laser-like operation for entangled photons.

Using multi-pass amplification pumped by higher-intensity pulses it should be possible to produce rotationally symmetric multi-photon entangled states with an average photon (pair) number of the order of 100. As exploration of such states is based on post-selection, the challenge of creating them should go in parallel with the challenge of constructing low-loss transmission lines and high-efficiency multi-photon detectors. Although there are encouraging developments in low-loss optical fibres<sup>29</sup> and highly efficient multi-photon detectors<sup>30</sup>, we will always have to face the situation of losing photons in the process of creating, transporting and analysing the desired state of equation (2). As this state is one large, complex, entangled state, one might think that the loss (or a measurement) of a single photon would destroy all the interesting properties of the state. On the contrary, the complex entanglement has the remarkable feature that the loss or measurement of one (or more) particles does not eliminate all the entanglement between the remaining particles. To illustrate this point, we focus our attention on the 4-photon state of equation (4), and consider a measurement of a photon in mode  $a$  in the H/V basis, with the measurement result being H. The state of the remaining three particles will be  $(1/\sqrt{2})|1,0;0,2\rangle - |0,1;1,1\rangle$ , which still contains non-maximal entanglement between modes  $a$  and  $b$ . A generalization to the actual loss of several photons from the full state (2) is currently under study.

The increased sharpness of the peaks in the interference pattern for the singlet of spin-1 (see Fig. 4) is potentially of interest for applications in metrology. An interferometric measurement of relative distance, for example, would benefit from the more precise

location of the maxima obtained by looking at the 4-fold (or higher) coincidence rates. Furthermore, the increased amount of entangled terms made available by stimulated emission and post-selection offer new possibilities for higher-bit-rate quantum cryptography. We consider that entanglement robustness—together with the rotational symmetry of the state created by stimulated polarization entanglement—opens the way to many applications in quantum information, and provides a powerful tool for studying the almost unexplored area between the discrete and the macroscopic optical quantum correlation experiments. □

Received 2 May; accepted 3 July 2001.

- Clauser, J. F. & Shimony, A. Bell's theorem: experimental tests and implications. *Rep. Prog. Phys.* **41**, 1881–1927 (1978).
- Aspect, A., Dalibard, J. & Roger, G. Experimental test of Bell's inequalities using time-varying analyzers. *Phys. Rev. Lett.* **49**, 1804–1807 (1982).
- Ou, Z. Y. & Mandel, L. Violation of Bell's inequality and classical probability in a two-photon correlation experiment. *Phys. Rev. Lett.* **61**, 50–53 (1988).
- Shih, Y. H. & Alley, C. O. New type of Einstein-Podolski-Rosen experiment using pairs of quanta produced by optical parametric down-conversion. *Phys. Rev. Lett.* **61**, 2921–2924 (1988).
- Tittel, W., Brendel, J., Zbinden, H. & Gisin, N. Violation of Bell inequalities by photons more than 10 km apart. *Phys. Rev. Lett.* **81**, 3563–3566 (1998).
- Wehls, G., Jennewein, T., Simon, C., Weinfurter, H. & Zeilinger, A. Violation of Bell's inequality under strict locality conditions. *Phys. Rev. Lett.* **81**, 5039–5043 (1998).
- Pan, J.-W. *et al.* Experimental test of non-locality in three-photon Greenberger-Horne-Zeilinger entanglement. *Nature* **403**, 515–519 (2000).
- Boumeester, D. *et al.* Experimental quantum teleportation. *Nature* **390**, 575–579 (1997).
- Boschi, D. *et al.* Experimental realization of teleporting an unknown pure quantum state via dual classical and Einstein-Podolski-Rosen channels. *Phys. Rev. Lett.* **80**, 1121–1125 (1998).
- Ekert, A., Rarity, J. G., Tapster, P. R. & Palma, G. M. Practical quantum cryptography based on two-photon interferometry. *Phys. Rev. Lett.* **69**, 1293–1295 (1992).
- Jennewein, T., Simons, C., Wehls, G., Weinfurter, H. & Zeilinger, A. Quantum cryptography with entangled photons. *Phys. Rev. Lett.* **84**, 4729–4732 (2000).
- Tittel, W., Brendel, J., Zbinden, H. & Gisin, N. Quantum cryptography using entangled photons and energy-time Bell states. *Phys. Rev. Lett.* **84**, 4737–4736 (2000).
- Slusher, R. E. *et al.* Observation of squeezed states generated by four-wave mixing in an optical cavity. *Phys. Rev. Lett.* **55**, 2409–2412 (1985).
- Wu, L. A., Kimble, H. J., Hall, J. L. & Wu, H. Generating squeezed states by parametric down-conversion. *Phys. Rev. Lett.* **57**, 2520–2523 (1986).
- Ou, Z. Y., Pereira, S. F., Kimble, H. J. & Peng, K. C. Realization of the Einstein-Podolski-Rosen paradox for continuous variables. *Phys. Rev. Lett.* **68**, 3663–3666 (1992).
- Furusawa, A. *et al.* Unconditional quantum teleportation. *Science* **282**, 706–709 (1998).
- Kwiat, P. G. *et al.* New high-intensity source of polarization-entangled photon pairs. *Phys. Rev. Lett.* **75**, 4337–4341 (1995).
- Kok, P. & Braunstein, S. L. Postselected versus non-postselected quantum teleportation using parametric down-conversion. *Phys. Rev. A* **61**, 042304-1–042304-10 (2000).
- Simon, C., Wehls, G. & Zeilinger, A. Optical quantum cloning via stimulated emission. *Phys. Rev. Lett.* **84**, 2993–2996 (2000).
- Ou, Z. Y., Rhee, J.-K. & Wang, L. J. Observation of four-photon interference with a beam splitter by pulsed parametric down-conversion. *Phys. Rev. Lett.* **83**, 959–962 (1999).
- Boumeester, D. *et al.* Observation of three-photon Greenberger-Horne-Zeilinger entanglement. *Phys. Rev. Lett.* **82**, 1345–1349 (1999).
- De Martini, F., Mussi, V. & Bovino, F. Schroedinger cat states and optimum universal quantum cloning by entangled parametric amplification. *Opt. Commun.* **179**, 581–589 (2000).
- DeMartini, F. & Di Giuseppe, G. Multiparticle quantum superposition and stimulated entanglement by parity selective amplification of entangled states. *Z. Naturforsch.* **56**, 61–66 (2001).
- Weinfurter, H. & Zukowski, M. Four photon entanglement from down conversion. Preprint quant-ph/0103049 at (<http://xxx.lanl.gov>) (2001).
- Knill, E., Laflamme, R. & Milburn, G. J. A scheme for efficient quantum computation with linear optics. *Nature* **409**, 46–52 (2001).
- Atature, M. *et al.* Partial distinguishability in femtosecond optical spontaneous parametric down-conversion. *Phys. Rev. Lett.* **83**, 1323–1326 (1999).
- Herzog, T. J., Rarity, J. G., Weinfurter, H. & Zeilinger, A. Frustrated two-photon creation via interference. *Phys. Rev. Lett.* **72**, 629–632 (1994).
- Milonni, P. W., Fearn, H. & Zeilinger, A. Theory of two-photon down-conversion in the presence of mirrors. *Phys. Rev. A* **53**, 4556–4566 (1996).
- Cregan, R. F. *et al.* Single-mode photonic band gap guidance of light in air. *Science* **285**, 1537–1539 (1999).
- Kim, J., Takeuchi, S. & Yamamoto, Y. Multiphoton detector using visible light photon counter. *Appl. Phys. Lett.* **74**, 902–904 (1999).
- Naik, D. S., Peterson, C. G., White, A. G., Berglund, A. J. & Kwiat, P. G. Entangled state quantum cryptography: eavesdropping on the Ekert protocol. *Phys. Rev. Lett.* **84**, 4733–4736 (2000).

## Acknowledgements

We thank C. Mikkelsen, P. Varisco, W. Irvine, A. Ekert and J. Rarity for suggestions and experimental support. This work was supported by the EPSRC, the UK Defence Evaluation and Research Agency, and the European QuComm project.

Correspondence and requests for materials should be addressed to A.L.-L. (e-mail: a.lamas@qubit.org).